







Coronal Cavities in CoMP Observations

Agnieszka Rumińska^{1,2} , Urszula Bąk-Stęślicka¹ , Sarah E. Gibson³ , and Yuhong Fan³ ¹Astronomical Institute, University of Wrocław, Wrocław, Poland; urszula.bak-steslicka@uwr.edu.pl²Department of Biological Sciences, University of Bergen, Norway³National Center for Atmospheric Research, Boulder, CO, USA

Received 2021 October 8; revised 2021 December 1; accepted 2021 December 22; published 2022 February 21

Abstract

Quiescent coronal cavities can provide insight into solar magnetic fields. They are observed in the coronal emission lines in both polarized and unpolarized light. In the total linear polarization fraction (L/I), they often possess a “lagomorphic,” or “rabbit-shaped,” structure that reflects the underlying magnetic field configuration. We studied quiescent coronal cavities observed between 2012 and 2018 by the Coronal Multichannel Polarimeter (CoMP). The majority of cavities in our study had a characteristic lagomorphic structure in linear polarization. We additionally compared cavity widths as observed in intensity with sizes of their linear polarization signatures for 70 cavities and found that both features are strongly correlated. Our results indicate that chances for observing a lagomorphic structure increase greatly with cavity lifetime, suggesting that the visibility depends on the spatial orientation of the cavity. Forward-modeled observations in linear polarization of flux ropes confirmed this assumption. We conclude that observations of the solar coronal cavities in linear polarization are consistent with the theoretical model of flux rope formation and structure.

Unified Astronomy Thesaurus concepts: [Quiescent solar prominence \(1321\)](#); [Quiet solar corona \(1992\)](#); [Solar magnetic fields \(1503\)](#)

1. Introduction

The classical three-part coronal mass ejection (CME) contains a bright front, dark cavity, and bright core associated with an erupting prominence (Illing & Hundhausen 1986; Tandberg-Hanssen 1995). A similar pattern is observed in the quiescent structure: a bright helmet streamer, an elliptical dark cavity, and a prominence. Such quiescent cavities may be long-lived and exist in equilibrium for many days or weeks (Gibson et al. 2006; Karna et al. 2017). Cavities are dark regions of rarefied density with elliptical cross sections (Gibson et al. 2006; Fuller & Gibson 2009; Forland et al. 2013; Gibson 2015) observed mostly in the polar crown regions (Tandberg-Hanssen 1995). Even quiescent cavities may finally erupt as a CME (Maričić et al. 2004; Vršnak et al. 2004; Gibson et al. 2006; Regnier et al. 2011).

Cavities were observed for the first time during the solar eclipse in 1898 (Wesley 1927), and since then, they have been analyzed many times (Von Klüber 1961; Williamson et al. 1961; Waldmeier 1970; Gibson et al. 2006). The first interpretation of a cavity as an area of reduced electron density was proposed in 1941 by Waldmeier (1941). Cavities are better visible outside the active region, with no bright, nearby structures (Gibson 2015; McCauley et al. 2015). They can be observed in a wide wavelength range, white light (Gibson et al. 2006), radio, extreme ultraviolet (EUV), and soft X-rays (Hudson et al. 1999; Hudson & Schwenn 2000; Marqué et al. 2002; Maričić et al. 2004; Heinzel et al. 2008; Berger et al. 2012; Reeves et al. 2012). Smaller cavities are quite visible in EUV, particularly in 193 Å (McCauley et al. 2015), while larger cavities are better revealed in white light (Gibson 2015).

The thermal properties of coronal cavities have been a subject of research by many authors (Guhathakurta et al. 1992; Hudson et al. 1999; Hudson & Schwenn 2000; Fuller et al. 2008; Vásquez et al. 2009; Habbal et al. 2010; Kucera et al. 2012; Reeves et al. 2012) addressing the question of whether cavities are hotter or cooler than their surroundings. Using the differential emission measure method, Bąk-Stęślicka (2019) analyzed 33 cavities and concluded that in every case, the cavity was hotter than the surrounding streamer. That work also found that the temperatures of both cavities and streamers vary as a function of different phases of solar activity.

Coronal cavities have been modeled as a flux rope (Low 1994; Low & Hundhausen 1995); however, their magnetic structure has been studied for many years (Gibson 2018, and references therein). Polarimetry gives the opportunity to distinguish between different models of the cavity: flux ropes, spheromak flux ropes, and sheared arcades (Rachmeler et al. 2013). In the previous paper, Bąk-Stęślicka (2013) used the Coronal Multichannel Polarimeter (CoMP; Tomczyk et al. 2008) measurements to obtain the direction of the magnetic field in the plane of the sky (POS) and analyzed the magnetic topology of quiescent prominence cavities. CoMP observed the solar corona via measurements of the forbidden lines of Fe XIII and provided information about line intensity, linear polarization, Doppler shift, and line width. Polarimetric observations revealed the common occurrence of a characteristic structure associated with cavities, which we called lagomorphic, due to their resemblance to rabbit heads. Those structures may be explained with the flux rope model (Bąk-Stęślicka 2013). Preliminary results revealed that the size of the CoMP lagomorphic signature scales with the cavity size seen in EUV (Bąk-Stęślicka 2014).

CoMP observations also revealed interesting structures in Doppler velocity. Schmit et al. (2009) showed, for the first time, line-of-sight (LOS) flows of coronal plasma within a coronal cavity. Bąk-Stęślicka et al. (2016) presented multiple



Original content from this work may be used under the terms of the [Creative Commons Attribution 4.0 licence](#). Any further distribution of this work must maintain attribution to the author(s) and the title of the work, journal citation and DOI.

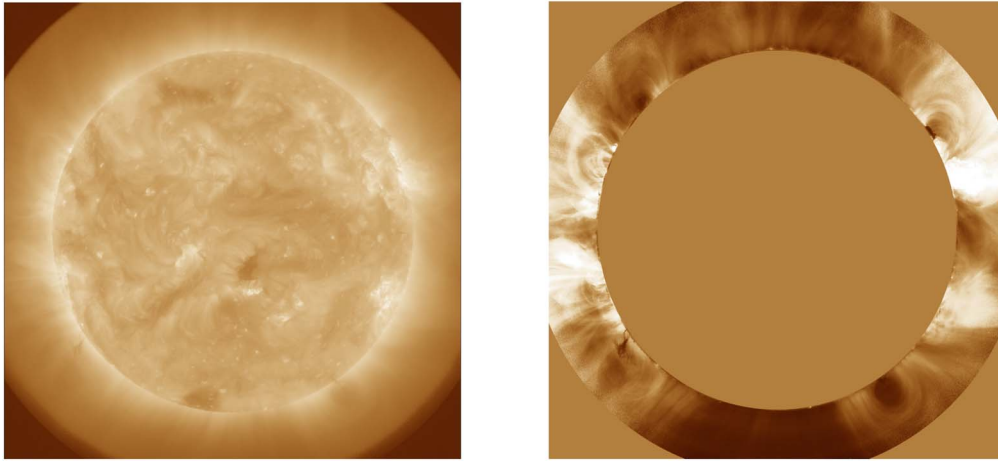


Figure 1. We applied a normalizing filter (NRGF) to visualize the structures in the solar corona. Left: the Sun recorded by SDO/AIA on 20.03.2012 (level 2 fits data). Right: filtered image of the solar corona, 20.03.2012 (displayed range: 1–1.37 R_{\odot}).

examples of such flows in the form of nested ringlike structures with counterstreaming velocities.

In this paper, we analyze cavities observed by the CoMP instrument between 2012 and 2018. We identify 1272 quiescent cavities and find that the majority of them possess a characteristic lagomorphic structure. In Section 2, we describe our data analysis. Our results and discussion are presented in Section 3. In Section 4, we give our summary.

2. Instrument and Data Analysis

2.1. Instruments

In our analysis, we used observations of the solar corona from the Atmospheric Imaging Assembly (AIA; Lemen et al. 2012) on board the Solar Dynamic Observatory (SDO; Pesnell et al. 2012). The AIA continuously makes full-disk images of the Sun through 10 passbands with a spatial resolution of $\approx 1''$, temporal cadence of 12 s, and field of view of at least $1.3 R_{\odot}$. The AIA consists of four telescopes and provides narrowband imaging of seven EUV bandpasses centered on the following emission lines: Fe XVIII (94 Å), Fe VIII, XXI (131 Å), Fe IX (171 Å), Fe XII, XXIV (193 Å), Fe XIV (211 Å), He II (304 Å), and Fe XVI (335 Å).

We also used polarimetric observations provided by CoMP, installed at the Mauna Loa Solar Observatory (MLSO) in Hawaii. The instrument made daily observations of the lower corona with a field of view of about 1.04 – $1.4 R_{\odot}$. Since 2010 October, CoMP has measured the magnetic field in the solar corona via the polarimetric signal (Stokes I , Q , U , V) in the forbidden lines of Fe XIII at 1074.7 and 1079.8 nm (Tomczyk et al. 2008). The circular polarization (Stokes V) provides information about the strength of the magnetic field along the LOS. Due to the very low intensity of the circular polarization signal, long integration times on the order of hours are required. Linear polarization has a much stronger signal and constrains the direction of the magnetic field in the POS.

2.2. Data Analysis

In a first step, we looked through MLSO/CoMP daily images and searched for dark, circular, or elliptical regions in the corona near the solar poles. We made a list of all cavities visible in CoMP intensity (CoMP I). We then looked at daily CoMP linear polarization images (CoMP L/I), seeking

coherent dark signatures with clear lagomorphic morphology in the region of the cavities. For images that were noisy, we processed median L/I images using the full set of CoMP images and adjusted the contrast. The L/I is the total linear polarization fraction, defined as $L/I = \sqrt{Q^2 + U^2}/I$. We used observations obtained between 2012 January and 2018 March. The observations are available at the MLSO website: https://mlso.hao.ucar.edu/mlso_data_calendar.php.

The CoMP repository contained one averaged image of the solar corona per day, with time resolution spanning a few hours of observations; we thus considered distinct observations as single data points. In order to calculate the actual number of *individual* cavities seen by CoMP (i.e., those with lifetimes longer than 1 day), we compared the observations with the SDO database. We used full-disk and solar corona images in the 193 Å wavelength. The SDO observations are available in the online repository: <https://sdo.gsfc.nasa.gov/data/aiahmi/>.

Since the SDO/AIA instrument observes the Sun at a cadence of 12 s, it was possible to track the evolution of coronal structures with good accuracy. We were therefore able to record the position and the beginning and end dates for each cavity. For practical reasons, the lifetime of each cavity was recorded in days instead of hours or minutes. After combining observations from these two instruments, we noted the number of days each cavity was visible in the Stokes I images and whether it had a lagomorphic structure visible in L/I .

Cavities are part of bigger, 3D systems (Gibson 2015) and often visible for many hours or even days at the same latitude, regardless of the rotation of the star. They can, however, be masked by, i.e., coronal loops or streamers and temporarily disappear from the image. Despite that, if the cavity reappeared in a similar position after some time, we considered it a separate event, even though it might have been a part of the same large-scale structure.

For further analysis, we selected cavities that have been observed by both instruments and had clear signatures in SDO/AIA 193 Å, CoMP I , and CoMP L/I images. We used level 1.5 fits files (*Quick Invert*) for CoMP data and level 2 fits files for SDO/AIA. To determine the center of each cavity, we used AIA 193 Å observations, since they have better image resolution compared to CoMP data (4096×4096 versus 602×620 pixels). It allowed us to find the cavity center with better accuracy and minimize measurement uncertainty. The procedure

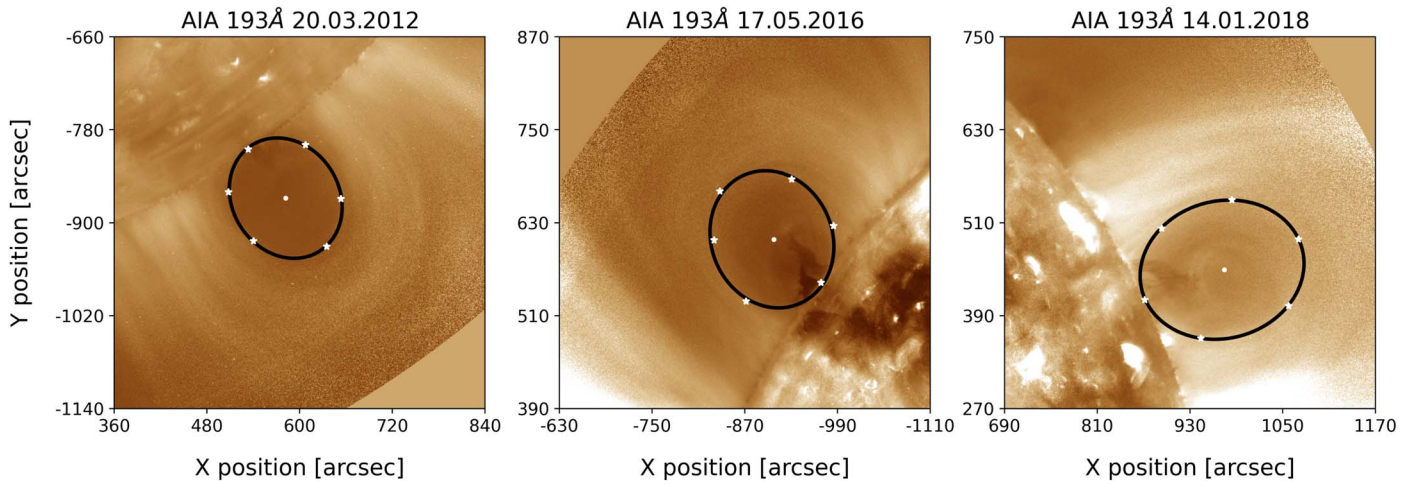


Figure 2. Three coronal cavities with fitted ellipses, observed on 20.03.2012, 17.05.2016, and 14.01.2018 (left to right). For each case, we manually selected points on the periphery of the cavity (marked with white stars), fitted an ellipse (black contours), and calculated the coordinates of its center (white dots).

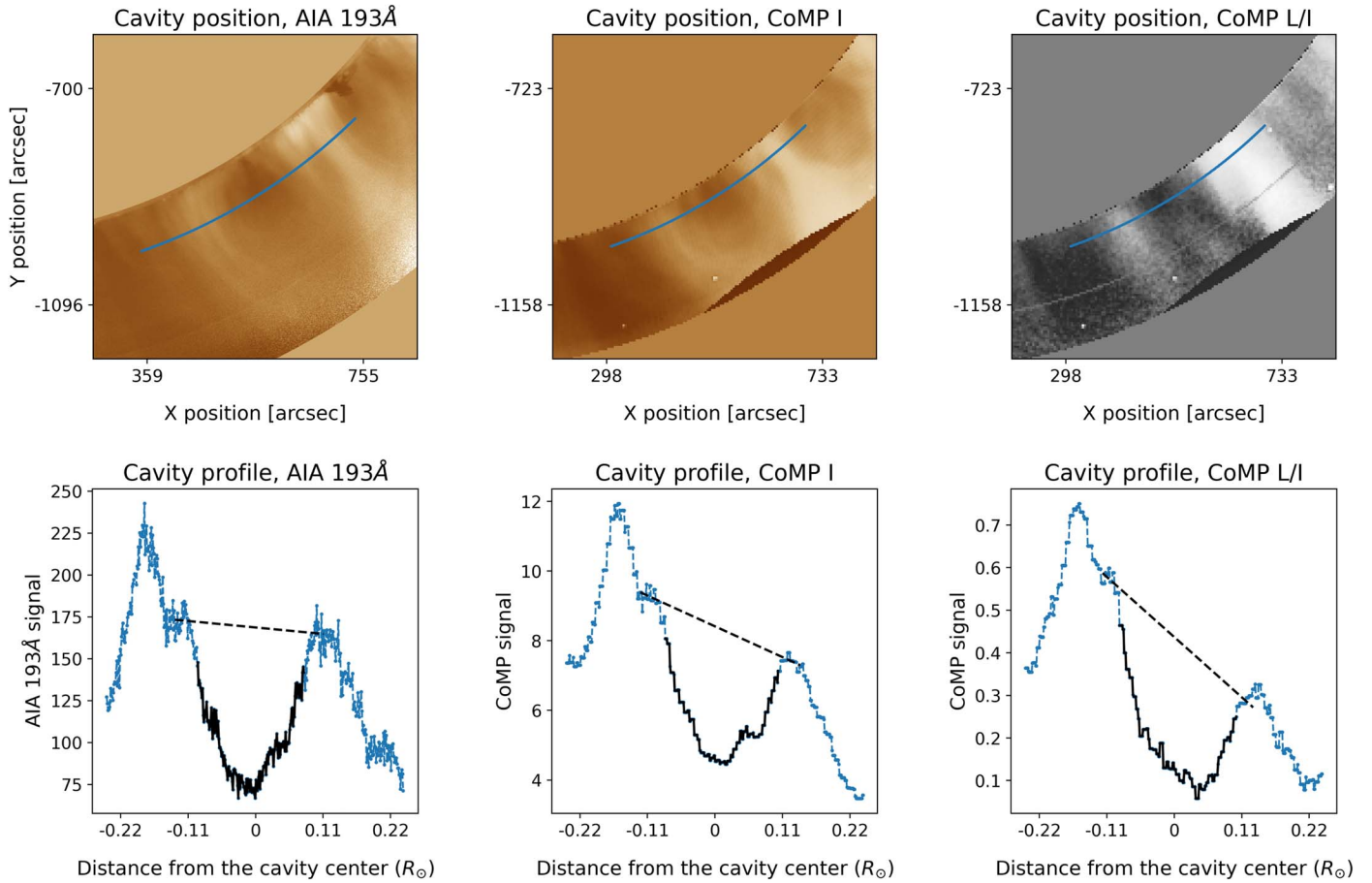


Figure 3. Upper panels: position of the coronal cavity observed on 15.12.2012 by SDO/AIA and CoMP (polar angle cuts are marked with blue lines). Lower panels: intensity profiles with significant signal drop indicating the position of a cavity. The black dashed line was fitted to the points on the edges. The width of a cavity was determined by an area where signal decreased more than 3σ in relation to the fitted line and is marked with solid black line. We used unfiltered (level 2 and *Quick Invert*) fits images to extract intensity profiles.

was similar to that described in Bąk-Stęślicka (2014) and Forland et al. (2013). We first applied a normalizing filter (Morgan et al. 2006) in order to enhance the contrast and visibility of the coronal structures (Figure 1). Using dedicated software in python, we manually selected points on the periphery

of each cavity, fitted an ellipse, and calculated the coordinates of its center (Figure 2). We assumed that the center of the ellipse correlates spatially with the cavity center projected on the POS. We repeated the procedure for each cavity three times to achieve reasonably accurate measurements. The true center of the cavity

Table 1
Summary of All Cavities Observed by CoMP from 2012 January to 2018 March

	2012	2013	2014	2015	2016	2017	I-III 2018	Total
Number of cavities in CoMP observations	213	289	97	209	91	315	58	1272
Number of cavities with L/I in CoMP observations	133	224	75	102	74	240	49	897
% of cavities with L/I	62%	76%	77%	49%	81%	76%	84%	71%

Table 2
Summary of All Individual Cavities Observed by CoMP from 2012 January to 2018 March

	2012	2013	2014	2015	2016	2017	I-III 2018	Total
Number of individual cavities in CoMP observations	91	96	51	91	52	151	32	564
Number of individual cavities with L/I in CoMP observations	70	85	47	63	44	127	27	463
% of cavities with L/I	77%	89%	92%	69%	85%	84%	84%	82%
CoMP observing days	250	228	242	200	128	284	50	1382

Note. Individual cavities are defined as cavities that have been observed continuously for few days, according to AIA data.

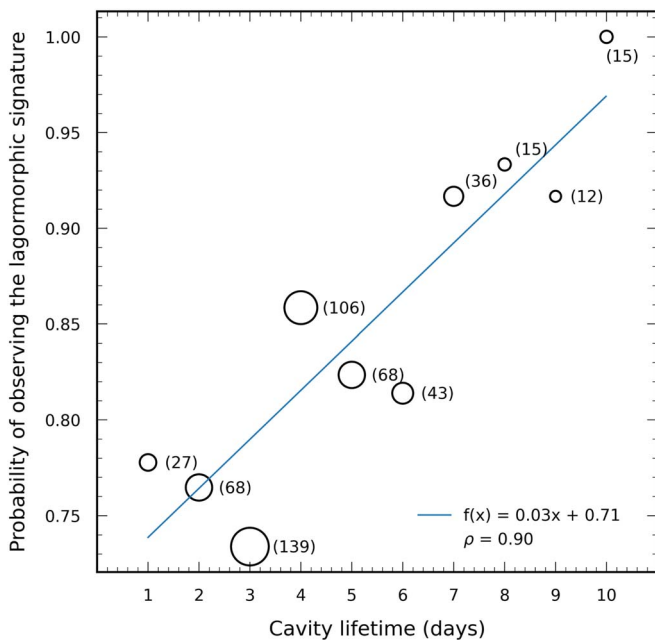


Figure 4. Probability of observing lagomorph structure as a function of cavity duration (in days). We analyzed 529 cavities from our data set that were visible for 1–10 days. We fitted a linear function and calculated correlation coefficient to check the dependency between variables. The probability of observing a lagomorph is strongly positively correlated with cavity lifetime ($\rho = 0.90$). The size of each circle and numbers provided in parentheses represent how many cavities were visible for a given number of days.

was approximated with the average of these measurements, with a standard deviation typically ranging between 1 and 5 pixels in each direction (along the x - and y -axes) on the POS.

We assumed that cavity height (expressed in R_{\odot}) did not change significantly for both instruments during the same observing day; therefore, we were able to determine the cavity center in CoMP images using simple geometric transformations. The procedure was performed on observations from the same date and hour to minimize the error caused by spatiotemporal dynamics of the analyzed structure and shifts in the cavity position.

To compare cavity width with the size of a lagomorph structure, we analyzed signal profiles through the cavity. The profiles were obtained by performing polar angle cuts in the

AIA 193 Å, CoMP I , and CoMP L/I images at the same height, corresponding to the cavity center calculated previously (Figure 3, upper panels). For each profile, we first calculated an average background signal by selecting points on both sides of the cavity and fitting a straight line using a least-squares approximation. We defined the cavity width using the area where the signal decreased more than 3σ in relation to the fitted line (Figure 3, lower panels). We repeated the analysis three times, each time selecting slightly different points on the periphery, and calculated a mean and standard deviation of the cavity width for each profile.

In Section 3, we present a comparison of cavity and corresponding lagomorph sizes for 70 cases. All cavities with centers lying below the CoMP occulter or too close to the occulter arm were excluded from our analysis. In order to avoid large uncertainties, we also excluded cavities for which the data included significant artifacts or the intensity profile had a poor signal-to-noise ratio.

Emergence of the structure in L/I depends on the angles between the local magnetic vector and the LOS (Rachmeler et al. 2013). We applied forward modeling to analyze how the visibility of the lagomorph structure in linear polarization depends on the orientation of the flux rope and to test the model predictions resulting from its internal magnetic structure. We used the MHD model of a prominence-carrying flux rope described in Fan & Liu (2019) and calculated synthetic observations in linear polarization based on the approach proposed by Gibson et al. (2016).

To illustrate how the condition of the polarimetric observations influences the chance of observing lagomorphs, we calculated the probability of seeing a lagomorph structure in the L/I images for 529 cavities. The probability is expressed as a proportion of days when the cavity was observed with a rabbit-shaped structure (extracted from the CoMP database) divided by the total number of days when the cavity was visible.

3. Results

We studied the occurrence of quiescent coronal cavities in 2012–2018 and their characteristics in polarized and unpolarized light. We also analyzed the link between cavity size and the size of a lagomorph structure in polarized light. In order to test the flux rope model for the magnetic field distribution inside the cavity, we performed a set of forward calculations to

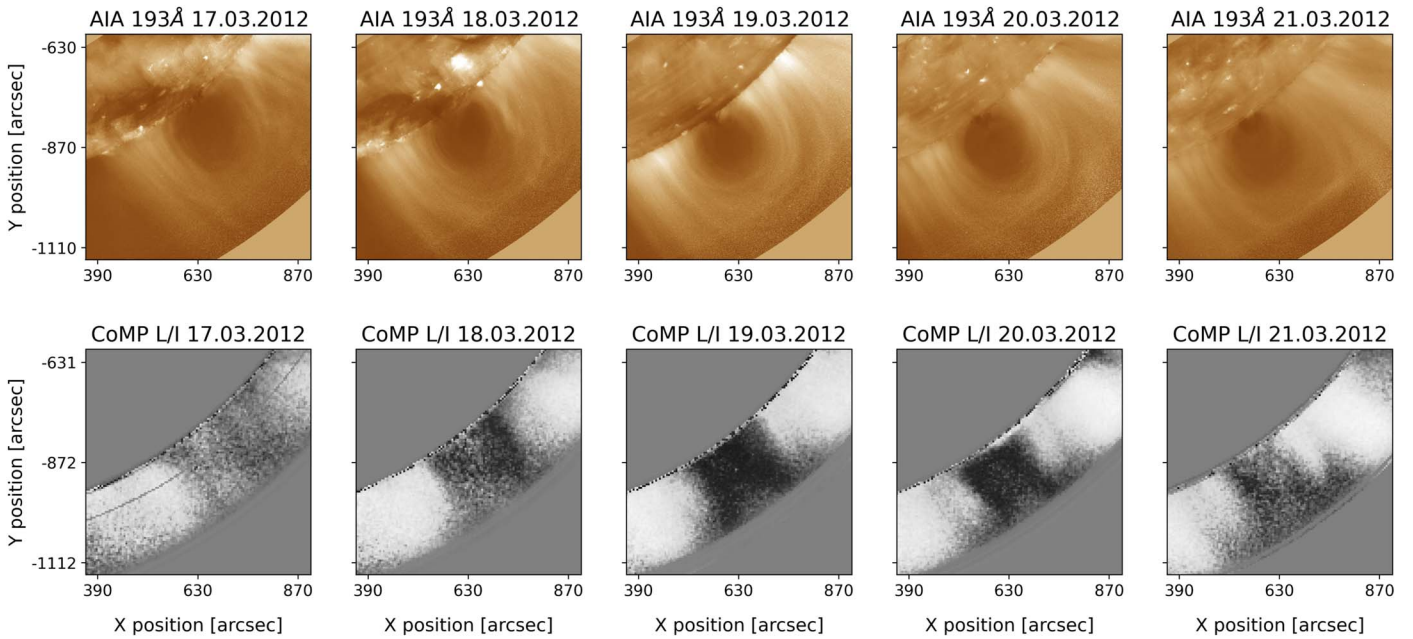


Figure 5. Coronal cavity observed between 2012 March 17 and 21 by SDO/AIA (upper panels) and corresponding observations in linear polarization (lower panels). The characteristic “lagomorph” structure in L/I was changing its shape, while the cavity remained stable.

examine how the orientation of an ideal cavity influences the chances of seeing a characteristic lagomorph structure.

3.1. Appearance of Cavities: Statistics

We obtained 1382 days of observations from the MLSO repository from 2012 January to 2018 March. In this period, CoMP observed 1272 coronal cavities, of which 71% had a visible lagomorph signature in L/I (Table 1).

Based on CoMP and SDO/AIA data, we identified 564 individual cavities, which are presented in Table 2, combined in annual intervals. We define individual cavities as cavities that have been observed continuously for 1 or more days, according to AIA data.

We found that about 82% (463) of all individual cavities had clearly visible, characteristic structures in linear polarization for at least 1 day (Table 2). The signature in L/I was usually not visible during the whole lifetime of the cavity. We therefore analyzed the probability of observing lagomorph structure as a function of cavity duration (in days) for 529 cases. We excluded from the analysis cavities that lasted for more than 10 days, since in our database, they were always identified with the L/I structure. The relation is presented in Figure 4. Cavities with longer lifetimes had higher probability of being observed by CoMP and therefore greater chances of being associated with lagomorph structures.

The probability of seeing a lagomorph structure for the longest-observed cavities (10 days or more) was 100%. The mean lifetime of a cavity was approximately 5 days. Cavities observed for 3 days were the most abundant in our database; in 2012–2018, there were as many as 136 such cavities.

It has previously been proposed that more cavities are visible when the Sun remains quiet, in contrast to periods with high solar activity (Gibson 2015; McCauley et al. 2015). The CoMP data did not cover the span of a whole solar cycle, but it is still possible to draw conclusions about general trends in the appearances of solar cavities. Our survey suggests that the relation between the number of cavities and solar activity indeed seems to be inversely proportional. We calculated how

many cavities, on average, were observed per day each year, near the maximum and minimum of solar cycle 24, and compared the results with yearly mean sunspot numbers. Both of these measures are simple arithmetic means of the daily total number of observed sunspots or cavities over all days in a year.

To provide accurate measurements, we chose the period around the solar maximum in which the monthly number of sunspots was the most stable. For 2012 and 2013, considerable fluctuations in solar activity were reported (Basu 2013). We therefore examined the appearances of cavities and sunspots in 2014, with a mean monthly sunspot number ≥ 90 for the whole period. We also chose 2017 as a proxy for solar minimum. The number of cavities observed during the maximum was about 0.40 day^{-1} , and that in the minimum was around 1.12 day^{-1} . During the same period, an average of 113.3 (maximum) and 21.7 (minimum) sunspots day^{-1} were observed. The information about sunspot numbers was accessed through the SILSO World Data Center (2021).

3.2. Forward-modeled Flux Rope

Even though a single cavity can be observed for many days, we are usually not able to see its characteristic signature in the L/I images for the whole time. The cavity observed between 2012 March 17 and 2021 March 21, presented in Figure 5, is a good example. There are several possible factors that influence the chances of detecting lagomorph structures: changing the position of the cavity in the POS, a change in the orientation of the cavity axis as the Sun rotates, or poor quality of data obtained from the instrument. In this section, we focus on investigating how the orientation of a flux rope influences the formation of a lagomorph structure in polarimetric observations by applying forward modeling.

Bąk-Stęślińska (2013) interpreted such characteristic lagomorph structures using forward modeling (Gibson et al. 2016 and references therein). That work used the isothermal MHD model of Fan (2010) and calculated synthetic observations in linear polarization. It concluded that the observations were consistent with the flux rope model.

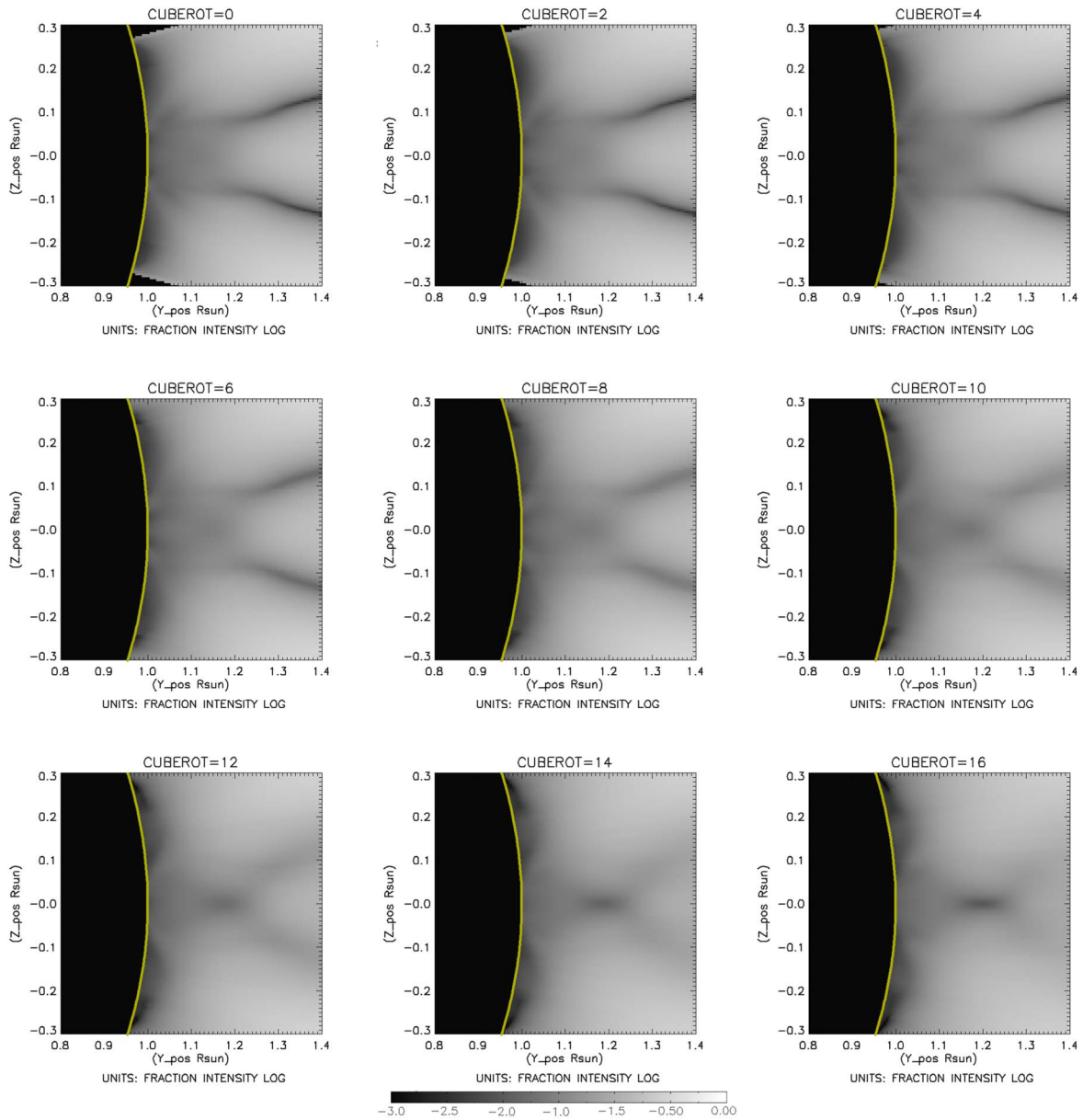


Figure 6. The LOS-integrated Stokes L/I for the forward-calculated 3D flux rope model. The edge of the solar disk is indicated by the curved yellow line. The first panel presents a nonrotated model. Other models present rotated structure in the range 2° – 16° .

The magnitude of linear polarization depends on the angle θ between the direction of the local magnetic field and the LOS ($L \propto \sin^2 \theta$, where $L = \sqrt{Q^2 + U^2}$ is the total linear polarization). Characteristic lagomorphic structures, where the signal is unpolarized, are visible due to the Van Vleck effect (creating the rabbit’s ears) and the magnetic field aligned along the LOS (creating the rabbit’s head); see Rachmeler et al. (2013) and Bąk-Stęślicka (2013). In case of low-lying cavities, the rabbit’s head might not be visible due to the occulter.

In this paper, we use the MHD simulation of a prominence-carrying flux rope by Fan & Liu (2019) and apply forward modeling to answer the question of whether a lagomorphic structure will be visible if the orientation of the magnetic flux rope changes. We rotated the magnetic flux rope axis by 1° relative to the LOS and calculated synthetic observations in linear polarization. We repeated this approach 20 times up to 20° rotation from the LOS. Figure 6 shows the forward-modeled Stokes L/I for several angles of rotation (0° , 2° , 4° ,

6° , 8° , 10° , 12° , 14° , and 16°). We can see that the lagomorphic structure is visible if the magnetic flux rope is rotated by less than 15° from the LOS. It may explain why lagomorphic structures are not visible for a number of cavities in our study.

3.3. Cavity Widths

Bąk-Stęślicka (2014) presented an initial test of whether the width of the cavity and the size of the lagomorph are comparable. The aim of the present work is to extend that study and provide detailed information about the sizes of the coronal cavities observed by CoMP. In the analysis, we included 70 coronal cavities that have been observed between 2012 January and 2018 March by CoMP and SDO/AIA and for which observations in total linear polarization were available.

First, we calculated and compared cavity widths in unpolarized UV and IR light. Figure 7 (top panel) shows the relationship between cavity widths observed by SDO/AIA

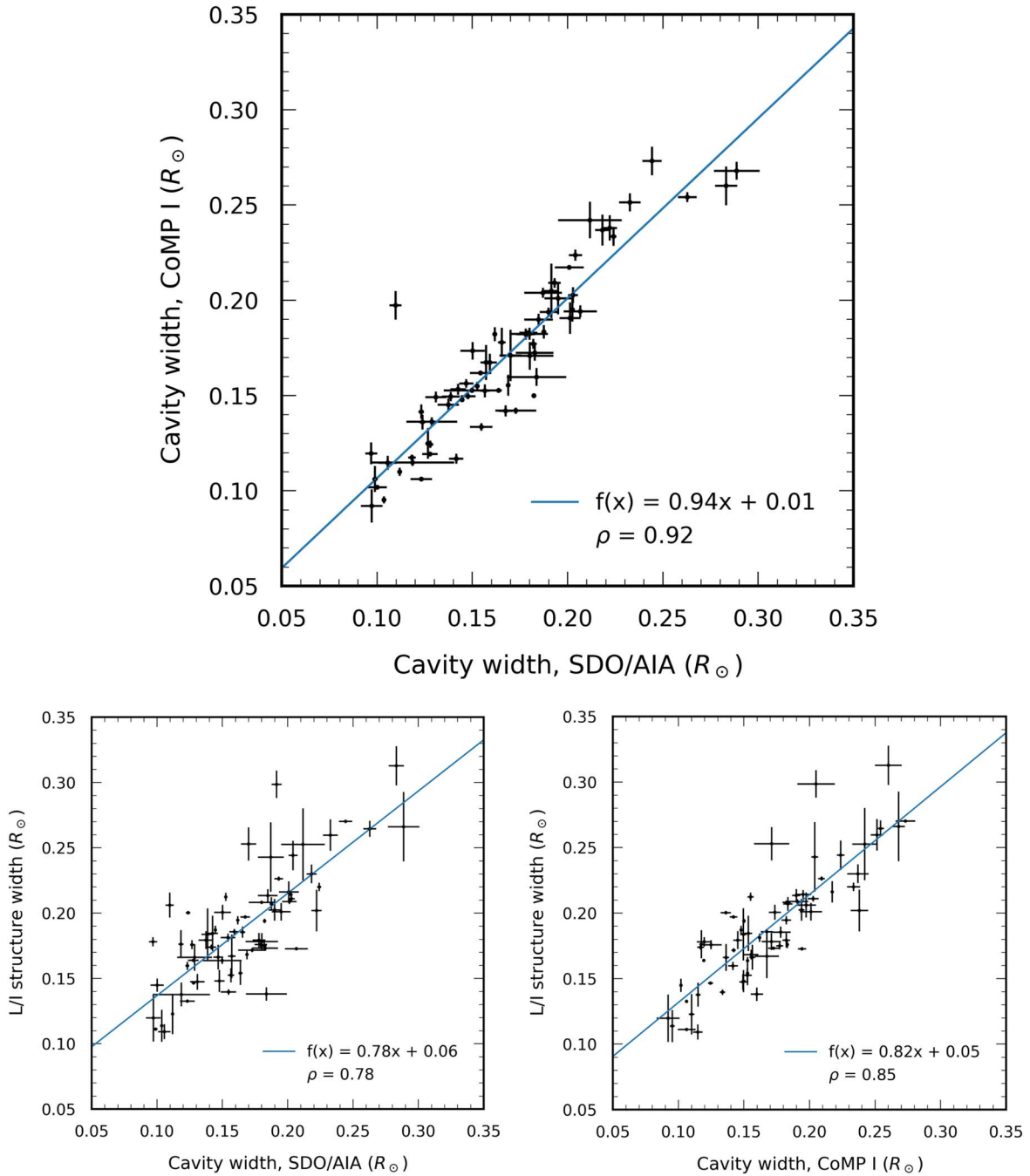


Figure 7. Top: cavity widths observed by SDO/AIA plotted against cavity widths observed by CoMP. Bottom left: cavity widths observed by SDO/AIA plotted against the sizes of their lagomorphic structures. Bottom right: cavity widths observed by CoMP plotted against the sizes of their lagomorphic structures. A sample contains 70 cavities.

through the 193 \AA filter and cavity widths observed by CoMP in the 1074 nm band (total intensity, CoMP I). A linear function was fitted to the points using a least-squares method. We obtained high positive correlation between the two widths ($\rho = 0.92$), meaning that the sizes of the cavities in UV and IR light are comparable. Cavity sizes in our study, measured in the POS, ranged from about 0.10 to $0.30 R_{\odot}$. The standard deviation for each width measurement did not exceed 10%.

We applied the same method for calculating the sizes of the lagomorphic structures (as described in Section 2.2 and Figure 3) and compared them with corresponding cavity widths measured in CoMP I and SDO/AIA observations. The

results are presented in Figure 7 (bottom panels). We fitted a linear function to each observation and calculated correlation coefficients. In both cases, we obtained a high positive correlation ($\rho = 0.85$ and 0.78 , respectively) between the variables, indicating that the size of a lagomorph indeed depends on the observed cavity width.

4. Summary

We studied the appearances of quiescent coronal cavities during several years of observations. We focused on analyzing the signal in polarized light (total fraction of linearly polarized

light, L/I) and combined our results with synthetic observations obtained from a model proposed by Fan & Liu (2019).

We identified 1272 cavities observed by CoMP between 2012 and 2018. About 71% of them were associated with characteristic lagomorphic structures described in Bąk-Stęślicka (2013). We combined the CoMP data with observations provided by SDO/AIA to find the number of individual cavities and their lifetimes. Among all individual quiescent cavities ($n = 564$), 82% had a lagomorphic structure in total linear polarization. Our study shows that the likelihood of observing a lagomorphic structure increases greatly with cavity duration, suggesting that under ideal conditions, it would probably be observed for every cavity.

We additionally performed measurements of cavity widths and sizes of lagomorphic structures for a sample of 70 cavities selected from our data set. We used polar angle cuts in the AIA 193 Å, CoMP I , and CoMP L/I images and obtained signal profiles at heights corresponding to the center of each cavity. Using signal profiles, we determined the width of the cavity seen on AIA 193 Å and CoMP I images and the width of the structure seen in linear polarization. The widths of the cavities observed through different filters (IR and EUV) are strongly correlated ($\rho = 0.92$). Our research also confirmed the initial assumption that the size of the cavity scales with the size of the lagomorphic structure ($\rho = 0.85$).

Polarimetric observations with CoMP were biased due to long integration times and unstable weather conditions. We therefore applied forward modeling to obtain synthetic observations in linear polarization and further investigate under what conditions a lagomorphic structure can be seen. We assumed a magnetic flux rope model and rotated the structure in steps by several degrees. Our analysis indicates that the lagomorphic structure became invisible when the cavity was rotated more than 15° with respect to the observer's LOS.

While observations of the solar corona in polarized light can serve as an important tool for measuring the orientation of a magnetic vector, their true value is revealed when combined with computer modeling. Integrating these two approaches allowed us to test theoretical assumptions about the structure of quiescent coronal cavities. We conclude that the chances of detecting a lagomorphic structure increase greatly with continuous coverage of the observation and a long lifetime of the cavity, which is indicative of an alignment of the cavity with the LOS. The above facts show that a lagomorphic structure is a typical signature of a cavity in polarized light and that the observations are in line with the assumed flux rope model of a cavity.

We thank Steven Tomczyk for internal review of this manuscript. The authors acknowledge helpful discussion with Arkadiusz Berlicki. The CoMP data were provided courtesy of the Mauna Loa Solar Observatory, operated by the High Altitude Observatory, as part of the National Center for Atmospheric Research (NCAR). The NCAR is a major facility sponsored by the NSF under cooperative agreement No. 1852977. Publication was partially financed by the program "Excellence Initiative—Research University" for the University of Wrocław.

ORCID iDs

Agnieszka Rumińska  <https://orcid.org/0000-0002-9536-4688>

Urszula Bąk-Stęślicka  <https://orcid.org/0000-0002-4014-3204>

Sarah E. Gibson  <https://orcid.org/0000-0001-9831-2640>

Yuhong Fan  <https://orcid.org/0000-0003-1027-0795>

References

- Basu, S. 2013, *JPhCS*, **440**, 012001
- Bąk-Stęślicka, U., Gibson, S. E., Chmielewska, E., et al. 2016, *FrASS*, **3**, 7
- Bąk-Stęślicka, U., Gibson, S. E., Fan, Y., et al. 2013, *ApJL*, **770**, L28
- Bąk-Stęślicka, U., Gibson, S. E., Fan, Y., et al. 2014, in *Nature of Prominences and their role in Space Weather*; Proc. of the IAU 300 (Cambridge: Cambridge Univ. Press), 395
- Bąk-Stęślicka, U., Gibson, S. E., Stęślicki, M., et al. 2019, *SoPh*, **294**, 1
- Berger, T. E., Liu, W., & Low, B. 2012, *ApJL*, **758**, L37
- Fan, Y. 2010, *ApJ*, **719**, 728
- Fan, Y., & Liu, T. 2019, *FrASS*, **6**, 27
- Forland, B., Gibson, S., Dove, J., Rachmeler, L., & Fan, Y. 2013, *SoPh*, **288**, 603
- Fuller, J., & Gibson, S. 2009, *ApJ*, **700**, 1205
- Fuller, J., Gibson, S., De Toma, G., & Fan, Y. 2008, *ApJ*, **678**, 515
- Gibson, S. 2015, *Solar Prominences* (Berlin: Springer), 323
- Gibson, S., Foster, D., Burkepile, J., De Toma, G., & Stanger, A. 2006, *ApJ*, **641**, 590
- Gibson, S. E. 2018, *LRSP*, **15**, 1
- Gibson, S. E., Kucera, T. A., White, S. M., et al. 2016, *FrASS*, **3**, 8
- Guhathakurta, M., Rottman, G., Fisher, R., Orrall, F., & Altrock, R. 1992, *ApJ*, **388**, 633
- Habbal, S. R., Druckmüller, M., Morgan, H., et al. 2010, *ApJ*, **719**, 1362
- Heinzl, P., Schmieder, B., Farník, F., et al. 2008, *ApJ*, **686**, 1383
- Hudson, H., Acton, L., Harvey, K., & McKenzie, D. 1999, *ApJL*, **513**, L83
- Hudson, H., & Schwenn, R. 2000, *AdSpR*, **25**, 1859
- Illing, R., & Hundhausen, A. 1986, *JGRA*, **91**, 10951
- Karna, N., Zhang, J., & Pesnell, W. 2017, *ApJ*, **835**, 135
- Kucera, T., Gibson, S., Schmit, D., Landi, E., & Tripathi, D. 2012, *ApJ*, **757**, 73
- Lemen, J. R., Akin, D. J., Boerner, P. F., et al. 2012, *SoPh*, **275**, 17
- Low, B. 1994, *PhPI*, **1**, 1684
- Low, B., & Hundhausen, J. 1995, *ApJ*, **443**, 818
- Maričić, D., Vršnak, B., Stanger, A., & Veronig, A. 2004, *SoPh*, **225**, 337
- Marqué, C., Lantos, P., & Delaboudiniere, J. 2002, *A&A*, **387**, 317
- McCauley, P. I., Su, Y., Schanche, N., et al. 2015, *SoPh*, **290**, 1703
- Morgan, H., Habbal, S. R., & Woo, R. 2006, *SoPh*, **236**, 263
- Pesnell, W. D., Thompson, B. J., & Chamberlin, P. 2012, *SoPh*, **275**, 3
- Rachmeler, L., Gibson, S., Dove, J., DeVore, C., & Fan, Y. 2013, *SoPh*, **288**, 617
- Reeves, K. K., Gibson, S. E., Kucera, T. A., Hudson, H. S., & Kano, R. 2012, *ApJ*, **746**, 146
- Regnier, S., Walsh, R., & Alexander, C. 2011, *A&A*, **533**, L1
- Schmit, D., Gibson, S., Tomczyk, S., et al. 2009, *ApJL*, **700**, L96
- 2021, SILSO World Data Center, S. 2014-2017, International Sunspot Number Monthly Bulletin and online catalogue, <https://www.bis.sidc.be/silso/>
- Tandberg-Hanssen, E. 1995, *The Nature of Solar Prominences*, 199 (Dordrecht: Kluwer Academic)
- Tomczyk, S., Card, G., Darnell, T., et al. 2008, *SoPh*, **247**, 411
- Vásquez, A. M., Frazin, R. A., & Kamalabadi, F. 2009, *SoPh*, **256**, 73
- Von Klüber, H. 1961, *MNRAS*, **123**, 61
- Vršnak, B., Maričić, D., Stanger, A., & Veronig, A. 2004, *SoPh*, **225**, 355
- Waldmeier, M. 1941, *Akad. Verlagsges* (Leipzig: Becker & Erler)
- Waldmeier, M. 1970, *SoPh*, **15**, 167
- Wesley, W. H. 1927, *Memoirs of the British Astronomical Association*, Vol. 64 (London: British Astronomical Association)
- Williamson, N., Fullerton, C., & Billings, D. 1961, *ApJ*, **133**, 973